Journal of Applied Mechanics Vol.12, pp.481-488 (August 2009) JSCE

Influence of particle shape on shear band formation of quasistatic granular media

Zafar MAHMOOD* and Kazuyoshi IWASHITA**

* PhD student, Dept. of Civil and Environmental Engineering, Saitama University
(255 Shimo Okubo, Sakura ku, Saitama, Japan)
** Member, Professor, Dept. of Civil and Environmental Engineering, Saitama University
(255 Shimo Okubo, Sakura ku, Saitama, Japan)

We study the influence of particle shape on the shear band formation in quasistatic granular media in biaxial compression test using two-dimensional Distinct Element Method (DEM). Elliptical-shaped particles are used to study the influence of particle shape. We also report an experimental verification to check the ability of DEM to model elliptical particles created by the clustering technique. It is observed in the experimental verification that DEM can model the elliptical particle. We simulate the shear band formation in biaxial compression test of granular media of elliptical particles using DEM. It is found that by using non-circular particles (e.g., elliptical in this study), generation of large voids and excess particle rotations inside the shear band are reproduced in a quite similar manner to those of the natural granular soils, which are difficult to produce with DEM model using circular particles unless rolling resistance used.

Key Words: *distinct element method, shear band, granular material, micromechanics*

1. INTRODUCTION

Granular materials present a complex mechanical response when subjected to an external load. This global response is strongly dependent on the discrete character of the medium. The shape, angularity and size distribution of the grains, the evolution of the granular skeleton (e.g., spatial arrangement of particles, void ratio, fabric, force chains), and some phenomena occurring at the grain scale (like rolling or sliding) are determinant factors for the overall macroscopic response.

Numerical simulations using Distinct Element Method (DEM) have become a valuable tool in the study of granular soil behavior from a micromechanical point of view. The method was introduced by Cundall and Strack[1] to model granular assemblies within the context of geotechnical engineering. DEM has the capability of modeling the material at the microscopic level and capture the entire phenomenon that pertains to the particulate nature of granular materials. The mechanical response of the granular media is obtained by modeling the particle interactions as a dynamic process and using simple mechanical laws in these interactions. Generally, discrete models use discs or spheres to reduce the time of calculation; however, these models do not consider the effect of particle shape on the mechanical behavior. Another discrepancy arising from the use of discs or spheres in numerical simulations is the excessive freedom of these particles to rotate compared with real soils. Various attempts have been made to address this phenomenon by constraining the rotation of circular particles[2),3)], or by using non-spherical/non-circular/arbitrary-shaped particles, e.g., elliptical-shaped particles in two-dimensional simulations[4),5)], ellipsoid-shaped particles in three dimensional simulations[6)], clusters of bonded discs/spheres[7–9)], clusters of overlapping discs[10),11)], and polygon shaped particles[12–16)].

The strain localization phenomenon and shear band formation is of great importance. To understand mechanics of shear band, many research works have been reported in past five decades in the field of soil mechanics[17–23)]. Furthermore, the strain localization problem is still a hot topic in the theoretical, as well as the experimental study of granular soil. The basic mechanism leading to shear band formation is still not understood well, despite these extensive studies.

The objectives of this study are: (a) to experimentally validate the ability of DEM to model the elliptical-shaped particles created by overlapping discrete circular elements (i.e., clustering technique); and (b) to investigate the effect of particle shape on strain localization, i.e., shear band formation. Two-dimensional DEM simulations of biaxial test are carried out to investigate the behavior of granular materials under monotonic loading. In order to include the effect of particle shape, elliptical-shaped particles, generated by clustering technique, are used.

2. MODELING NON-CIRCULAR PARTICLES

Any arbitrary-shaped particle can be modeled by considering the following points:

- The outline of an arbitrary-shaped particle can be achieved by a cluster of overlapping circles.
- The purpose of overlapping circles is to attain the shape of particle, and to detect contact among particles.
- Contact is not checked among the circles belonging to the same particle/cluster
- The kinematic restrictions are imposed on circles within a cluster to prevent relative rotation and translation.

3. NUMERICAL PROCEDURES

The simulations are carried out by means of Distinct Element Method (DEM). The DEM is based on the implicit time integration of the equations of motion. The details are given below.

3.1 Contact deformation

Consider two particles, a and b, in contact to which material reference points χ^a and χ^b are attached (Fig. 1). These reference points are located at positions $\boldsymbol{x}^a$ and $\boldsymbol{x}^b$ relative to the global axes. The vectors $\boldsymbol{r}^a$ and $\boldsymbol{r}^b$ connect points χ^a and χ^b to the contact. Branch vector $\boldsymbol{l}$ connects the two reference points: $\boldsymbol{l} = \boldsymbol{r}^a - \boldsymbol{r}^b = \boldsymbol{x}^a - \boldsymbol{x}^b$. The contact is assumed to be point like, with a contact area that is negligible compared to particle size. The particles undergo incremental translational and rotational movements $d\boldsymbol{u}^a$, $d\boldsymbol{u}^b$, $d\boldsymbol{\theta}^a$, and $d\boldsymbol{\theta}^b$ during time increment dt. In classical kinematics, the particles may be truly rigid, and, hence, prevented from inter-penetration, but the behavior of granular materials is influenced by the local particle deformations at their contacts. The contact deformations $d\boldsymbol{u}^{def}$ are produced by the relative motions of the two material points, one on either side of the contact,

$$d\boldsymbol{u}^{def} = (d\boldsymbol{u}^b - d\boldsymbol{u}^a) + (d\boldsymbol{\theta}^b \times \boldsymbol{r}^b - d\boldsymbol{\theta}^a \times \boldsymbol{r}^a)\,. \qquad (1)$$

This displacement is referred to as a contact deformation, and can be separated into components that are tangent and normal to the contact surface, producing sliding and indentation respectively. The contact deformation (Eq. 1) has long been used in the analysis and simulation of granular media.

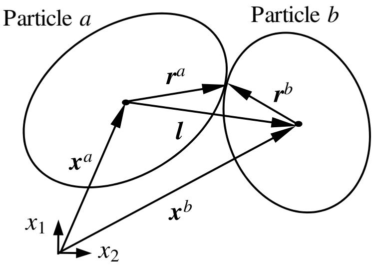

Fig. 1. Two particles in contact.

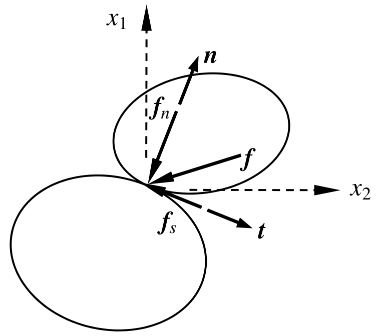

Fig. 2. Vectors and forces associated with the contact point between two grains.

3.2 Contact model

Fig. 2 shows vectors and forces associated with the contact point between two grains. Unit vector $\boldsymbol{n}$ is the unit contact normal and $\boldsymbol{t}$ is the unit vector tangent to the contact. Unit vector $\boldsymbol{t}$ is obtained by a clockwise rotation of $\boldsymbol{n}$ through 90°.

In conventional Distinct Element Method (DEM) each contact is replaced by a set of springs, dash pots, no-tension joints, and a shear slider, which responds to a contact force f acting on it (Fig. 2). The normal contact force, f_n, and tangential contact force, f_s, must be balanced against the resistance supplied by the springs and dash pots

$$f_n = k_n u_n + C_n \frac{du_n}{dt} \;\; ; \;\; f_s = k_s u_s + C_s \frac{du_s}{dt} \qquad (2)$$

where k_n and k_s are the stiffness constants of the normal and shear springs; and C_n and C_s are the coefficients of viscous damping of the normal and shear dash pots, respectively.

The shear slider starts working at any contact, as soon as f_s and f_n satisfy the following inequality:

$$|f_s| \geq \mu f_n \qquad (3)$$

where μ is the coefficient of friction. If the contact is purely cohesive with no frictional resistance, then the right hand side can by replaced by a constant c.

3.3 Stress

The average stress tensor[24),25)] acting on a granular assembly can be computed as

$$\sigma_{ij} = \frac{1}{V}\sum_{\alpha=1}^{N_c} f_i^{\alpha} l_j^{\alpha} \tag{4}$$

where f_i^{α} is the ith component of the contact force acting at the αth contact point between the two particles; l_j^{α} is the jth component of the branch vector connecting the centroid of two particles forming the αth contact point; and N_c is the total number of contacts in the volume V. A contact is created when it transmits contact force f.

If an assembly of volume V is subjected to external forces T_i^1, T_i^2,…, T_i^m on its boundary points x_i^1, x_i^2,…, x_i^m; the average stress of an equivalent continuum of the same volume V under the same loads is [26]

$$b_{ij} = \frac{1}{V}\sum_{\beta=1}^{m} T_i^{\beta} x_j^{\beta} \tag{5}$$

where b_{ij} is referred to as the boundary stress.

As shown by Tu and Andrade[27], the balance of linear momentum in granular assembly is ensured if $\boldsymbol{\sigma} = \boldsymbol{b}$, and balance of angular momentum is ensured if $\boldsymbol{\sigma} = \boldsymbol{\sigma}^T$.

4. EXPERIMENTAL VALIDATION

In order to check the ability of DEM to model the elliptical-shaped particles (created by clustering technique), an experimental verification is discussed in this section.

An experimental validation program was carried out by: (a) building an experimental setup that allows tracking the translation and rotation of model grain resulting from an external disturbance; (b) numerically simulating the experimental setup using DEM with the same initial conditions and material properties; and (c) comparing the experimental and numerical results.

4.1 Experimental program

Two-dimensional elliptical-shaped particle made of plastic and aspect ratio 1.5 was chosen as a model grain for the experimental verification. As shown in Fig. 3, the experimental boundary conditions were defined by a horizontal box and a piston, where a single elliptical particle of dimensions 48 × 32 mm and 10 mm in thickness was placed with different initial inclinations (i.e., δ = 0, 30, 45, 60°). The piston was 50 × 20 × 300 mm. The elliptical particle was displaced by moving the piston (Fig. 3). To measure the particle movement with a particle tracking method, two marks were placed at equal distance from the center on the major axis of elliptical particle. A mark was placed on the piston to measure its displacement.

A high speed video camera (FASTCAM-X 1280 PCI, frame rate in this experiment: 1,000 frames per sec) connected with a frame grabber was set up vertically and was focused onto the apparatus to record the particle and piston movement. The positions of particle and piston in the recorded digital video frames were tracked by a particle tracking software "Dipp-Motion XD". Coordinates of two marks on the particle were mapped at each frame and used to evaluate the instantaneous position, and rotation of particle. The coordinates were recorded in pixels, and then converted into physical coordinates (for the condition of the experiment, there were 21.7 pixels per cm).

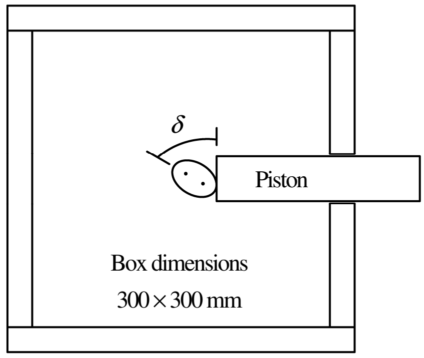

Fig. 3. Schematic diagram of experimental setup.

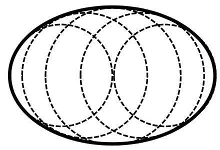

Fig. 4. Elliptical particle generated by overlapping 5 circles.

4.2 Numerical results

The experimental setup was simulated by using two-dimensional Distinct Element Method. The box was simulated as four fixed rigid walls, whereas the piston was simulated as a rigid wall that moved at a constant velocity. The piston movement was slow enough to ensure a stable solution. The model elliptical particle of aspect ratio 1.5 (with the same dimensions as used in the experiment) was generated by overlapping 5 circles (Fig. 4). A static friction working between the particle and floor may be incorporated in the simulations; however, we used a damping coefficient to account for the friction between the particle and floor. Another damping coefficient was used to account for dissipation of the particle's rotational energy.

The density of the simulated particle was set to the actual particle's density (i.e., 1.243 g/cm^3). The contact normal/shear stiffness was set to 10^5 N/m and the increment time step (Δt) of 10^{-6} sec was used.

4.3. Comparison

Validation experiment was carried out with different initial inclinations. Each validation experiment was repeated several times in order to study the inherent variability of the procedure due to slight changes in initial conditions. Particle displacement and inclination versus piston displacement both in the experiment and simulation are shown in Fig. 5 for the initial angle $\delta = 45^o$. From a qualitative and quantitative standpoint, it is clear that there is a good agreement between numerical simulation results and experimental results; therefore, DEM can model non-circular/ elliptical particles.

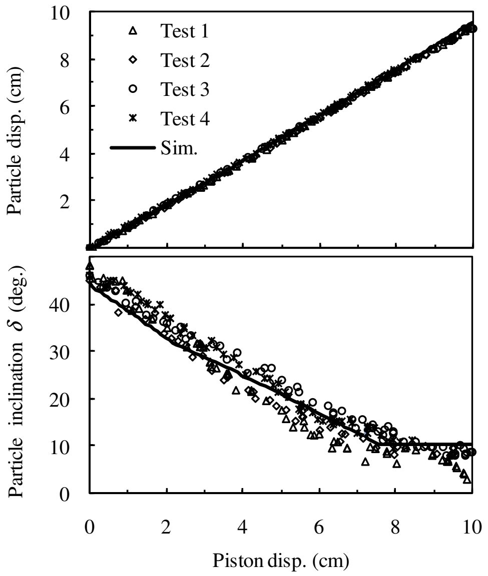

Fig. 5. Particle displacement and inclination plotted against piston displacement in experiment and simulation.

5. BIAXIAL SIMULATION TEST AND THEIR RESULTS

In this section, we describe two-dimensional DEM simulations of biaxial test and their results. In order to include the effect of particle shape, elliptical-shaped particles, generated by clustering technique , are used.

5.1. Preparation of particle assembly

The assembly was prepared by using three different size elliptical particles (i.e., large, medium and small, as in Table 1). The elliptical particles were generated by overlapping 5 circles (Fig. 4). The assembly of 27 *cm* × 54 *cm* consisted of 6,629 particles. The assembly was prepared by placing particles at random and was consolidated by applying uniform stress (p_0 = 200 kPa) on the four boundaries until oscillation of stress disappeared. The initial void ratio at the end of consolidation was 0.1254. The final assembly after the consolidation is shown in Fig. 6. For convenience, orthogonal reference axes x_i (i=1,2) were chosen as follows: x_1 is in the vertical direction and x_2 is in the lateral direction.

Mechanical properties of the assembly depend totally on physical constants dealing with contact behavior such as normal and shearing stiffness values. Choice of these constants is of great importance, in particular, when results from simulation tests are compared with those from real laboratory test quantitatively. In spite of this fact, most of these constants were tentatively chosen on an empirical basis as shown in Table 2. We can do this since our present objective is to investigate qualitatively the effect of particle shape on stress-strain behavior and micro-process of shear band development.

Table 1: Dimensions of particles

Description	Axial ratio	Dimensions (mm)
Large	1.5	7.5 × 5.0
Medium	1.5	6.0 × 4.0
Small	1.5	4.5 × 3.0

Table 2: Physical constants and experimental conditions in the simulation test

DEM parameters and material properties	Selected value
Number of particles	6,629
Increment of time step (Δt)	1.0×10^{-6} sec
Particle density	2,600 kg/m^3
Confining pressure	200 kPa
Friction coeff. between particles	0.49
Friction coeff. between particles and wall	0.36
Cohesion between particles (c)	0.0 N
Normal spring constant (k_n)	1.0×10^8 N/m
Tangential spring constant (k_s)	1.0×10^7 N/m
Damping constant at the contact	0.07

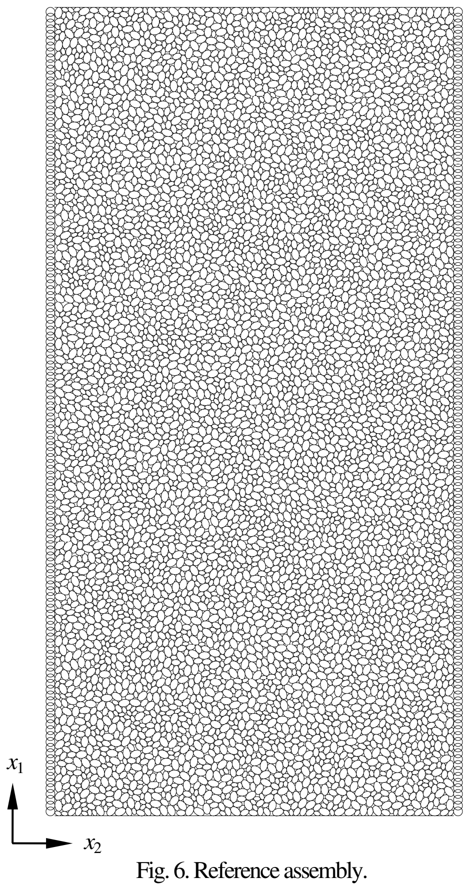

Fig. 6. Reference assembly.

Deformation of the particle assembly was controlled through four boundaries: top, bottom, left and right boundaries. The top and bottom boundaries moved vertically as loading platens under strain-controlled condition. To generate a shear band at a central portion of the assembly, friction was applied to interfaces between inside particles and the top and bottom platens (friction coefficient = 0.36).

The left and right boundaries, which are composed of circular particles (3 mm in radius) linked in chain, are flexible and can even stretch or shrink like a membrane. No friction worked between the inside particles and the membrane particles. End particles in the membrane were restricted so as to move together with the top and bottom boundaries in the vertical direction. However, they could move freely in the horizontal direction. Physical constants and properties of membrane- membrane particle interaction are shown in Table 3.

Table 3: Physical constants and properties of membrane-membrane particle interaction

Material properties	Selected value
Type of membrane particle	Circular
Diameter of membrane particle	3.0 mm
Normal spring constant (k_n)	1.0×10^6 N/m
Tangential spring constant (k_s)	0 N/m
Damping constant at the contact	0

5.2. Stress-strain relations

To run a biaxial test, two horizontal walls at top and bottom of the assembly were used to apply vertical stress σ_{11} with constant velocity (strain-controlled loading) while, a lateral stress σ_{22} ($=p_o$) was applied to the sample through flexible membrane. The average stresses σ_{11} and σ_{22} were calculated using Eq. 4. The global axial strain was calculated as $\varepsilon_{11} = \Delta H/H_0$, where H_0 is the initial height of the sample; ΔH is the change in height of sample. The global volumetric strain was calculated as $\varepsilon_V = \Delta V/V_0$, where V_0 is the initial volume of the sample; ΔV is the change in volume of sample. The volume was calculated by considering the area occupied by the top and bottom platens and taking into account the bulging of membrane. Note that these globally defined quantities lose their physical meaning if strain localization starts.

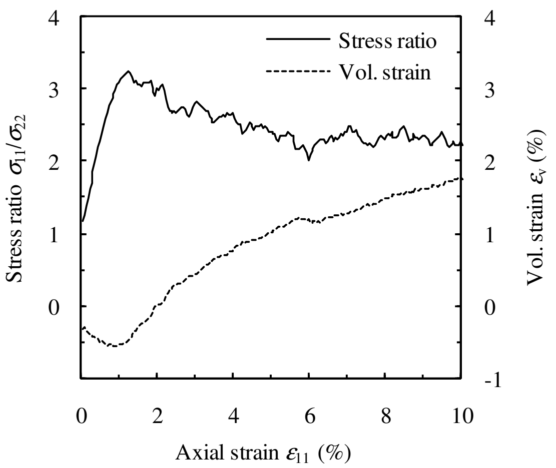

Fig. 7. Axial stress-strain-volumetric strain relation.

Fig. 7 shows the relationships between stress ratio σ_{11}/σ_{22}, global axial strain ε_{11} and global volumetric strain ε_V. We observe a classical behavior characterized by a hardening behavior followed by softening and a stress plateau corresponding to the residual state of soil mechanics. The volumetric strain is first compressive and followed by dilatancy. Since this kind of volumetric change is quite common in natural sands, one may infer that the deformation mechanism here is similar to that for natural sands, at least in a qualitative sense. The process of densification ceases just before peak stress ratio and then followed by dilatancy.

5.3. Volumetric strain

Lagrange's (local) strain tensor was calculated to examine more precisely progressive accumulation of volumetric strain in the assembly[28]. The local volumetric strain increments calculated at centers of all particles were assigned to these particles as shown in Fig. 8. White particles denote expansive volumetric strain, while black ones denote compressive volumetric strain by more than threshold value (0.5% in Figs. 8a, 8b and 2.0% in Figs. 8c, 8d) and others are omitted. The following are worth noting to understand what is going on inside a shear band.

Note, in Fig. 7, that global volumetric strain ε_V is compressive during the global deformation from $\varepsilon_{11} = 0$ to 0.91 % (i.e., before reaching peak) and then becomes dilative before reaching failure. As seen in Fig. 8a, the local volumetric strain increment is compressive. More importantly, it is distributed uniformly all over the assembly without concentration into some specific zones. This is typical one taking place during the so-called strain hardening process.

When the global strain ε_{11} reaches 1.28 %, the specimen fails. Fig. 8b shows that local volumetric strain increment is dilative during global deformation from ε_{11} = 0.91 to 1.28 % and locations where dilation occurs are limited to a certain zone only, suggesting that localization process has initiated. It means that local volumetric strain turns out to be dilative and concentrates into a certain zone before reaching the failure i.e., the onset of shear banding is a pre-peak phenomenon. Under plane strain conditions, shear banding has been most commonly observed to initiate during hardening[23),29–32)].

Softening occurs from global strain ε_{11} = 1.28 to 2.55% and extensive dilatancy is observed in the shear band as shown in Fig. 8c.

The assembly reaches a residual state at ε_{11}= 2.55 to 3.55%. The local volumetric strain is continuously concentrated into the shear band only at this stage; however, both compression and dilatancy occur simultaneously as seen in Fig. 8d.

The dilatational volumetric strain is concentrated, especially after failure, into the narrow shear bands, and that the strain softening behavior must be the result of weakening along such bands. Similar results have been reported in the numerical simulations of shear band formation in granular media consisting of circular particles, using modified distinct element method (MDEM) incorporating the rolling resistance [2),3),28)].

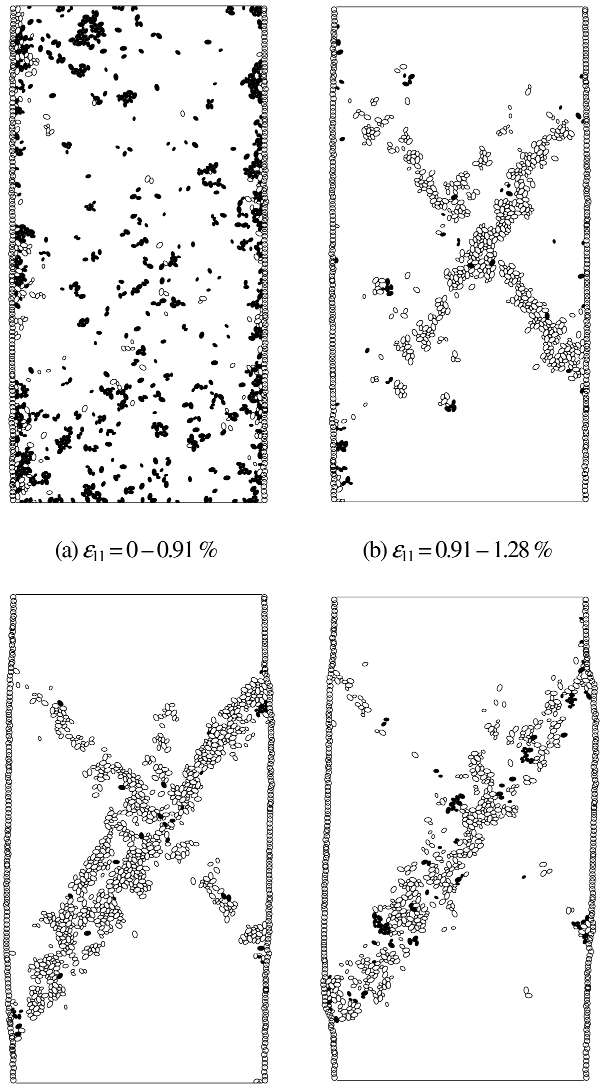

(a) $\varepsilon_{11} = 0 - 0.91$ %　(b) $\varepsilon_{11} = 0.91 - 1.28$ %

(c) $\varepsilon_{11} = 1.28 - 2.55$ %　(d) $\varepsilon_{11} = 2.55 - 3.55$ %

Fig. 8. Distribution of volumetric strain increment. White particles denote expansive volumetric stain while black particles denote compressive volumetric strain.

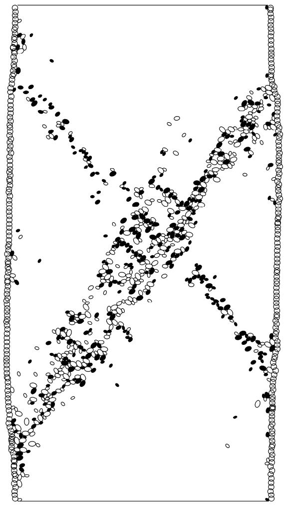

Fig. 9. Distribution of highly rotated particles during strain increment $\varepsilon_{11} = 0 - 3$ % White particles denote counterclockwise rotation by more than 15^{o} while black particles denote clockwise rotation by more than 15^{o}.

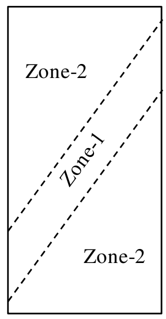

Fig. 10. Schematic zones in the reference assembly: zone-1 includes shear band, while zone-2 lies outside the shear band.

5.4 Particle rotation

It is well known that particle rotation plays a dominant role in the development of shear bands in granular assemblies as reported by Oda and Kazama[21)] in their experimental results on Toyoura and Ticino sands, and numerical simulations[2),3),28)]. Fig. 9 shows the particle rotation which took place during the global strain increment from ε_{11}= 0 to 3.0 %. The black particles rotated counterclockwise by more than 15^{o}, while white ones rotated clockwise by more than 15^{o}. Others are omitted. Note that particles rotate significantly in some limited zones. Counterclockwise rotation mainly occurs in shear band running from upper right to lower left, while clockwise rotation occurs in the conjugate shear band.

The absolute average rotation $|\bar{\theta}|$ of a specimen made of n particles is defined as

$$\left|\bar{\theta}\right| = \frac{1}{n}\sum_{i=1}^{n}\left|\theta_i\right| . \tag{6}$$

The reference assembly is divided into two zones: zone-1 includes the shear band, while zone-2 lies outside the shear band (Fig. 10). The boundaries of zone-1 are fixed to contain the excessively rotating particles observed at large axial strain. Fig. 11 shows the absolute average particle rotation in zone-1 and -2 (i.e., inside and outside the shear band respectively). The value of $|\bar{\theta}|$ both in zone-1 and-2 are the same till peak stress ratio; however, $|\bar{\theta}|$ increases abruptly at higher rate in zone-1 (i.e., inside the shear band) after the peak stress, whereas, $|\bar{\theta}|$ is very small outside the shear band till end of test.

5.5 Discussion

It is clear from the simulation test that large voids and particle rotations are concentrated in the shear band. Oda and Kazama[21)] observed large voids and excessive particle rotations concentrating in the shear band in biaxial compression test on real sands. Iwashita and Oda[2),3)] and Oda and Iwashita[28)] also reported that generation of large voids inside a shear band and a high gradient of particle rotation along the shear band boundaries can be reproduced by their rolling resistance model which was found difficult to simulate with circular particles using standard DEM. By using non-circular particles (e.g., elliptical in this study), we simulated the shear band formation using standard DEM model, which suggests that rolling resistance may be attributed to the particle shape.

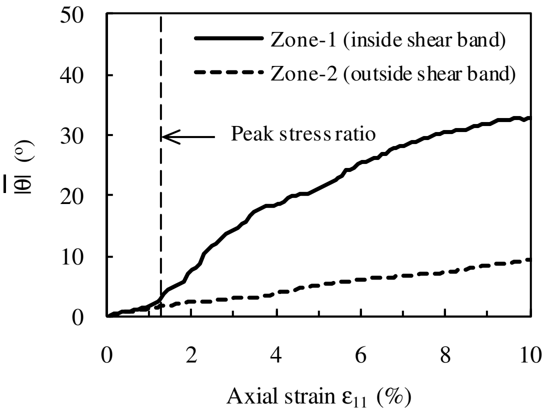

Fig. 11. Absolute average particle rotation inside and outside the shear band.

6. CONCLUSION

The conclusions summarized as follows:

(1) We carried out an experimental verification to check the ability of DEM to model the movement of elliptical-shaped particles created by overlapping discrete circular elements. The experimental setup consisted of a piston that could slide into a box to disturb an elliptical particle with pre-specified initial inclination. The movement of particle in the experiment was captured by high-speed camera and a particle tracking method. A numerical simulation of the experimental test was carried out by using two-dimensional DEM. A good agreement existed between experimental and numerical results.

(2) Two-dimensional DEM simulations of biaxial test were carried out to simulate the microstructure developed in shear bands. In order to include the effect of particle shape, elliptical-shaped particles, generated by clustering technique, were used. It was observed that generation of large voids and concentration of excessive particle rotations were found in the shear band in a quite similar manner to those of natural granular soils. The volumetric strain was found to start concentrating into the shear band immediately before the peak stress state, i.e., already in the hardening regime.

(3) Standard DEM model cannot simulate the development of shear band with circular particles unless rolling resistance used[2),3),21)]. By using non-circular particles (e.g., elliptical in this study), we simulated the shear band formation using standard DEM model, which suggests that rolling resistance may be attributed to the particle shape.

ACKNOWLEDGEMENTS

This work has been supported by Japan Society for Promotion of Science (JSPS), Grant-in-Aid for Scientific Research, Grant Number 18560482, 2006. Financial support to the first author provided by the Japanese Ministry of Education, Culture, Sports, Science and Technology (MEXT) is greatly acknowledged. The experimental validation carried out by Mr. Saitou Yuu, the undergraduate student of Saitama University, is gratefully acknowledged.

REFERENCES

1) Cundall, P.A., Strack O.D.L.: A discrete numerical model for granular assemblies, *Geotechnique*, Vol. 29, pp. 47–65, 1979.
2) Iwashita, K., Oda, M.: Rotational resistance at contacts in simulation of shear band development by DEM, *ASCE J. Engineering Mechanics*, Vol. 124, pp. 285–292, 1998.
3) Iwashita, K., Oda, M.: Micro-deformation mechanism of shear banding process based on modified distinct element method, *Powder Technology*, Vol. 109, pp. 192–205, 2000.
4) Ting, J.M., Khwaja, M., Meachum, L.R., Rowell, J.D.: An ellipse-based discrete element model for granular materials, *Int. J. Numer. Anal. Methods Geomech*., Vol. 17, pp. 603–623, 1993.
5) Ng, T-T.: Numerical simulations of granular soil using elliptical particles, *Computer and Geotechnics*, Vol. 16, pp. 153–169, 1994.
6) Lin, X., Ng, T-T.: A three-dimensional discrete element model using arrays of ellipsoids, *Geotechnique*, Vol. 47, pp. 319–329, 1997.
7) Jensen, R.P., Bosscher, P.J., Plesha, M.E., Edil, T.B.: DEM simulation of granular media-structure interface: effects of surface roughness and particle shape, *Int. J. Numer. Anal. Meth. Geomech.*, Vol. **23**, pp. 531–547, 1999.
8) Thomas, P.A., Bray, J.D.: Capturing nonspherical shape of granular media with disk clusters, *ASCE J. Geotech. Geoenviron. Engrg*., Vol. **125**, pp. 169–178, 1999.
9) Powrie, W., Ni, Q., Harkness, R.M., Zhang, X.: Numerical modeling of plane strain tests on sands using a particulate approach, *Geotechnique*, Vol. **55**, pp. 297–306, 2005.
10) Ashmawy, A.K., Sukumaran, B., Hoang, V.V.: Evaluating the influence of particle shape on liquefaction behavior using discrete element method, *Proceedings of the 13th International offshore and Polar Engineering Conference, Honolulu, Hawai, USA*, pp. 542–549, 2003.
11) Sallam, A.M.: Studies on modeling angular soil particles using the discrete element method, *Ph.D. Thesis*, University of South Florida, USA, 2004.
12) Mirghasemi, A., Rothenburg, L., Matyas, E.: Influence of particle shape on engineering properties of assemblies of

two-dimensional polygon-shaped particles, *Geotechnique*, Vol. 52, pp. 209–217, 2002.

13) Azema, E., Radjai, F., Peyroux, R.: Force transmission in a packing of pentagonal particles, *Physical Review E*, Vol. 76, pp. 011301, 2007.
14) Nouguier-Lehon, C., Cambou, B., Vincens, E.: Influence of particle shape and angularity on the behaviour of granular materials: a numerical analysis, *Int. J. Numer. Anal. Meth. Geomech.*, Vol. 27, pp. 1207–1226, 2003.
15) Alonso-Marroquin, F., Luding, S., Herrmann, H.J., Vardoulakis, I.: Role of the anisotropy in the elastoplastic response of a polygonal packing. *Physical Review E*, Vol. 51, pp. 051304, 2005.
16) Pena, A.A., Lizcano, A., Alonso-Marroquin, F., Herrmann, H.J.: Biaxial test simulations using a packing of polygonal particles, *Int. J. Numer. Anal. Meth. Geomech.*, Vol. 32, pp. 143–160, 2008.
17) Newland, P.L., Allely, B.H.: Volume changes in drained triaxial tests on granular materials, *Geotechnique*, Vol. 7, pp. 17–34, 1957.
18) Rowe, P.W.: The stress-dilatancy relation for static equilibrium of an assembly of particles in contact, *Proc., Royal Soc.*, Vol. A269, pp. 500–527, 1962.
19) Matsuoka, H.: Stress-strain relationship of sands based on the mobilized plane, *Soils and Foundations*, Vol. 14, pp. 47–61, 1974.
20) Nemat-Nasser, S.: On behavior of granular materials in simple shear, *Soils and Foundations*, Vol. 20, pp. 59–73, 1980.
21) Oda, M., Kazama, H.: Microstructure of shear bands and its relation to the mechanisms of dilatancy and failure of dense granular soils, *Geotechnique*, Vol. 48, pp. 465–481, 1998.
22) Alshibli, K.A., Batiste, S.N., Sture, S.: Strain localization in sand: plane strain versus triaxial compression, *J. Geotech. Geoenviron. Engrg.*, Vol. 129, pp. 483–494, 2003.
23) Rechenmacher, A.L.: Grain-scale processes governing shear band initiation and evolution in sands, *Journal of Mechanics and Physics of Solids*, Vol. 54, pp. 22–45, 2006.
24) Christoffersen, J., Mehrabadi, M.M., Nemat-Nasser, S.: A micromechanical description of granular material behavior, *J. Appl. Mech.*, Vol. 48, pp. 339–344, 1981.
25) Rothenburg, L., Selvadurai, A.P.S.: A micromechanical definition of the Cauchy stress tensor for particulate media, *Proceedings of the international symposium on the mechanical behavior of structured media*, Ottawa, ed. Selvadurai, Part B, pp. 469–486, 1981.
26) Drescher, A., de Josselin de Jong, G.: Photoelastic verification of a mechanical model for the flow of a granular material, *J. Mech. Phys. Solids*, Vol. 20, pp. 337–351, 1972.
27) Tu, X., Andrade, J.E.: Criteria for static equilibrium in particulate mechanics computations, *Int. J. Numer. Meth. Engng.*, Vol. 75, pp. 1581–1606, 2008.
28) Oda, M., Iwashita, K.: Study on couple stress and shear band development in granular media based on numerical simulation analyses, *International Journal of Engineering Science*, Vol. 38, pp. 1713–1740, 2000.
29) Desrues, J., Lanier, J., Stutz, P.: Localization of the deformation in tests on sand sample, *Eng. Fract. Mech.*, Vol. 21, pp. 909–921, 1985.
30) Han, C., Vardoulakis, I.: Plane-strain compression experiments on water-saturated fine-grained sand, *Geotechnique*, Vol. 41, pp. 49–78, 1991.
31) Finno, R.J., Harris, W.W., Mooney, M.A., Viggiani, G.: Shear bands in plane strain compression of loose sand, *Geotechnique*, Vol. 47, pp. 149–165, 1997.
32) Desrues, J., Viggiani, G.: Strain localization in sand: an overview of the experimental results obtained in Grenoble using sterophotgrammetery, *Int. J. Numer. Anal. Methods Geomech.*, Vol. 28, pp. 279–321, 2004.

(Received: April 9, 2009)